Solar RRL
www.solar-rrl.com

# In Situ 2D Perovskite Formation and the Impact of the 2D/3D Structures on Performance and Stability of Perovskite Solar Cells

*Matheus S. de Holanda, Rodrigo Szostak, Paulo E. Marchezi, Luís G. T. A. Duarte, José C. Germino, Teresa D. Z. Atvars, and Ana F. Nogueira**

**Hybrid organic and inorganic perovskite solar cells lack long-term stability, and this negatively impacts the widespread application of this emerging and promising photovoltaic technology. Herein, aiming to increase the stability of perovskite films based on $CH_3NH_3PbI_3$ and to deeply understand the formation of 2D structures, solutions of alkylammonium chlorides containing 8, 10, and 12 carbons are introduced during the spin-coating on the surface of 3D perovskite films leading to the in situ formation of 2D structures. It is possible to identify the chemical formulae of some 2D structures formed by X-ray diffraction and UV–vis analysis of the modified films. Interestingly, the increase in the stability of the $CH_3NH_3PbI_3$ films due to the formation of a 2D + 3D perovskite network is only possible in planar $TiO_2$ substrates. The increase in stability of the $CH_3NH_3PbI_3$ films follows the surfactant molecule order: octylammonium (8C) > decylammonium (1 °C) > dodecylammonium (12C) chlorides > standard. An increase of 17.6% in the lifetime of the devices assembled with octylammonium-modified perovskite film is observed compared with that of the standard device, which is directly linked to the improvement of the charge carrier lifetimes obtained from time-correlated single photon counting measurements.**

## 1. Introduction

Perovskite solar cells (PSCs) have attracted the attention of the scientific and industrial communities with records of power conversion efficiency (PCE) higher than 23%.[1,2] Perovskite is a class of materials with the crystalline structure of the calcium titanate and general formula $ABX_3$. Most of the perovskite-based semiconductors for application in photovoltaic devices can be considered as a hybrid, organic–inorganic perovskite, where the A site can be $CH_3NH_3^+$ (MA = methylammonium), $HC(NH_2)_2^+$ (FA = formamidinium), $Cs^+$, $Rb^+$; B site is $Pb^{2+}$ in most of the cases and $X^-$ is a halide anion ($Cl^-$, $Br^-$, $I^-$), being $CH_3NH_3PbI_3$ the most studied composition. Several characteristics make this material very interesting for applications in photovoltaics, as its bandgap can be tuned according to composition, temperature, and pressure; electron-hole diffusion length above 1000 nm; high absorption coefficient (higher than Si and GaAs), and the relatively low cost associated with wet chemical preparation and roll-to-roll deposition methods.[3–11] Despite these exceptional characteristics, this thin film semiconductor is unstable at ambient conditions, which can hinder a wide-scale production and future commercialization. Organic–inorganic hybrid perovskites present a strong affinity to water, resulting in an intense degradation when the material is subjected to environmental conditions with a high relative humidity.[12–14] Up to certain moisture conditions (RH ≤30%), the degradation process is reversible, and several studies indicate that the water molecules might be passivating the surface defects and grain boundaries.[15,16] However, at higher moisture conditions, this process is completely irreversible with the formation of mono and dehydrated structures ($CH_3NH_3PbI_3{\cdot}H_2O$ and $(CH_3NH_3)_4PbI_6{\cdot}2H_2O$, respectively) and subsequent formation of $PbI_2$ and $CH_3NH_3I$, according to the following mechanism.[17]

$$CH_3NH_3PbI_3 + H_2O \rightleftharpoons CH_3NH_3PbI_3 \cdot H_2O \quad (1)$$

$$4CH_3NH_3PbI_3 \cdot H_2O \rightleftharpoons (CH_3NH_3)_4PbI_6 \cdot 2H_2O + 3PbI_2 + 2H_2O \quad (2)$$

$$(CH_3NH_3)_4PbI_6 \cdot 2H_2O \rightarrow 4CH_3NH_3I + PbI_2 + 2H_2O \quad (3)$$

One of the approaches to increase the stability of organic–inorganic hybrid perovskites is the incorporation of bi-dimensional structures, such as the Ruddlesden–Popper phase $A'_2A_{m-1}B_mX_{3m+1}$, with A′ being an aromatic or aliphatic primary alkylammonium molecule.[18–23] These structures are commonly composed of $m$ repeated units of inorganic sheets of lead iodide corner shared octahedra. These sheets are sandwiched by monovalent alkylammonium molecules, called as separators. This type

M. S. de Holanda, R. Szostak, P. E. Marchezi, L. G. T. A. Duarte, Dr. J. C. Germino, Prof. T. D. Z. Atvars, Prof. A. F. Nogueira
Laboratório de Nanotecnologia e Energia Solar
Chemistry Institute
University of Campinas–UNICAMP
PO Box 6154, 13083-970 Campinas, São Paulo, Brazil
E-mail: anafla@unicamp.br

The ORCID identification number(s) for the author(s) of this article can be found under https://doi.org/10.1002/solr.201900199.

DOI: 10.1002/solr.201900199

 

of material has its properties tuned by layer thickness (number of repeating units of inorganic sheets, $m$), by the proportion between the salts of A′ and A used as precursors and by the barrier thickness or the distance between the layers that depends on the size of the surfactant.[18,24–27] The stability and formation energy of these materials also depend on the thickness of the layer and increases as thickness decreases.[26] The possibility to vary A′ allows the tuning of some important properties of these materials such as the bandgap, charge carrier mobility and diffusion, photoluminescence (PL), and wettability.[28] Recent studies have proven the advantage of these 2D perovskites in the increase of both PCE and tolerance toward moisture. The partial conversion of 3D to 2D structures was reported by Koh et al. and by Chen et. al. through the spin coating of butylammonium and octylammonium, on the first, and phenylethylammonium, and the last, iodides solution on 3D $Cs_{0.05}(MA_{0.17}FA_{0.83})Pb(I_{0.83}Br)_3$ thin films, leading to the formation of a surface layer composed of 2D structures.[29,30] Solar cells were also assembled using an interfacial mixture of 2D/3D perovskites by Grancini et al.; first by mixing methyammonium and aminovaleric acid ($HOOC(CH_2)_4NH_3^+$) iodides with lead iodide ($PbI_2$).[20] This approach made it possible to construct a sealed module with a stability of 10 000 h. In another work, Cho et al. used a fluorinated organic ammonium precursor in layer-by-layer deposition after the antisolvent process, which acts as a water-repellent interface for high efficient and stable PSCs (PCE = 20% under humidity at 500 h test).[31]

In this work, 2D structures were in situ formed in 3D methylammonium (MA) lead halide perovskite films, resulting in a 2D + 3D network. Long-chain aliphatic alkylammonium chloride ($C_mH_{2m+1}NH_3^+Cl^-$, $m = 8$, 10, 12) solutions were dripped on the surface of 3D perovskite films at the moment of deposition to form mixed structures. The surfactants were able to reorganize the bulk of $CH_3NH_3PbI_3$ leading to the formation of different 2D structures. We identified the chemical formulae of some of the 2D structures that were formed after the modification. The perovskite films were deposited on both planar and mesoporous $TiO_2$ films, and the impact on the stability depended on the type of the substrate. The resulting 2D + 3D mixed films were characterized by structural, microscopy, and photophysical techniques. They have shown to be more resistant to degradation, resulting in devices with improved stability, a feature correlated to the improvement of the charge carrier lifetime by the formation of 2D structures into the 3D perovskite framework.

## 2. Results and Discussion

**Figure 1**A shows the field emission scanning electron microscopy (FEG-SEM) images of the perovskite film surface with and without modification with the alkylammonium chloride surfactants. We observe the formation of a homogeneous granular perovskite film absent of pinholes in the standard $CH_3NH_3PbI_3$ film deposited over the planar $TiO_2$ substrate. The average grain size of the perovskite film is $178.5 \pm 73.28$ nm, and no changes in morphology could be seen after the treatment with the surfactant molecules. The same morphological characteristics are also observed when films were prepared on mesoscopic substrates (Figure S1a, Supporting Information). Cross-sectional images of the planar perovskite films were also obtained (Figure 1B). There is no significant variation in the film thickness of $585 \pm 25.6$ nm. Interestingly, changes in the morphology are now seen when comparing the perovskite films with and without the surfactants. The standard perovskite is composed of grains with a dimension smaller than the thickness of the film. However, the grains in the modified films are larger and with the same dimension of the thickness. We believe that the chloroform solvent promoted a slightly superficial dissolution of the perovskite film, allowing the surfactant to reorganize and form the 2D structures.[32,33] This is an indication of a total penetration of the surfactant solution into the perovskite film. As the surfactant length increases, the compactness also increases and larger grains are formed.[26,29] In addition to that, some works suggests that the presence of chloride may lead to the formation of larger grains, even that these ions do not remain on the films.[34,35]

The contact angle between a water drop and the surface of the perovskite films in the planar $TiO_2$ configuration was measured to get more information about the hydrophobicity of the surface after modification. The contact angle analysis (Figure 1C) confirms that the deposition of the surfactant results in a more hydrophobic surface. The increase in the chain length of the surfactant causes a decrease in the wettability of the film, indicating a surface more tolerant to the presence of moisture. The order of surface wettability is dodecylammonium < decylammonium < octylammonium < standard. This trend was also observed in the films deposited on the mesoscopic substrates (Figure S1b, Supporting Information).

Atomic force microscopy (AFM) images of the modified and standard perovskite films were also obtained (**Figure 2**A). In general, the introduction of the surfactant decreases the roughness of the perovskite films in comparision with the film without modification, as observed by the root mean square (RMS) values (23.5, 14.2, 18.8, and 21.6 nm for the standard, modified-octylammonium, modified-decylammonium, and modified-dodecylammonium films, respectively). According to Kelvin and atomic force microscopy (KPFM) analysis (Figure 2B), films modified with octylammonium and decylammonium exhibit regions with higher potentials, and we are inferring that these regions are composed of 2D structures, while the film modified with dodecylammonium present a surface potential distribution very similar to our standard film. The surfactants are expected to be bound to the surface $PbI_6^{-4}$ units via hydrogen bonds through ammonium ($R-NH_4^+$) groups and, eventually, penetrate on the perovskite crystallites, by the surface defects and grain boundaries, leading to the formation of 2D structures.[18,23,36] KPFM analysis corroborates with the FEG-SEM cross-sectional images that show that the bulk of the perovskite modified with dodecylammonium chloride results in a more compact film with larger grains. In this case, the resulting 2D structures seem to be more localized in bulk than at the surface. For the octylammonium and decylammonium modified films, the presence of 2D structures at the surface might be responsible for smoothing the perovskite surface. The RMS values calculated from the AFM topography images agree to the potential distribution, being the octylammonium-modified film the one with the smallest RMS value (14.2).

The X-ray diffraction (XRD) patterns of the perovskite films (**Figure 3**B) show almost complete conversion of the perovskite precursors after annealing. We observe only a low intensity peak

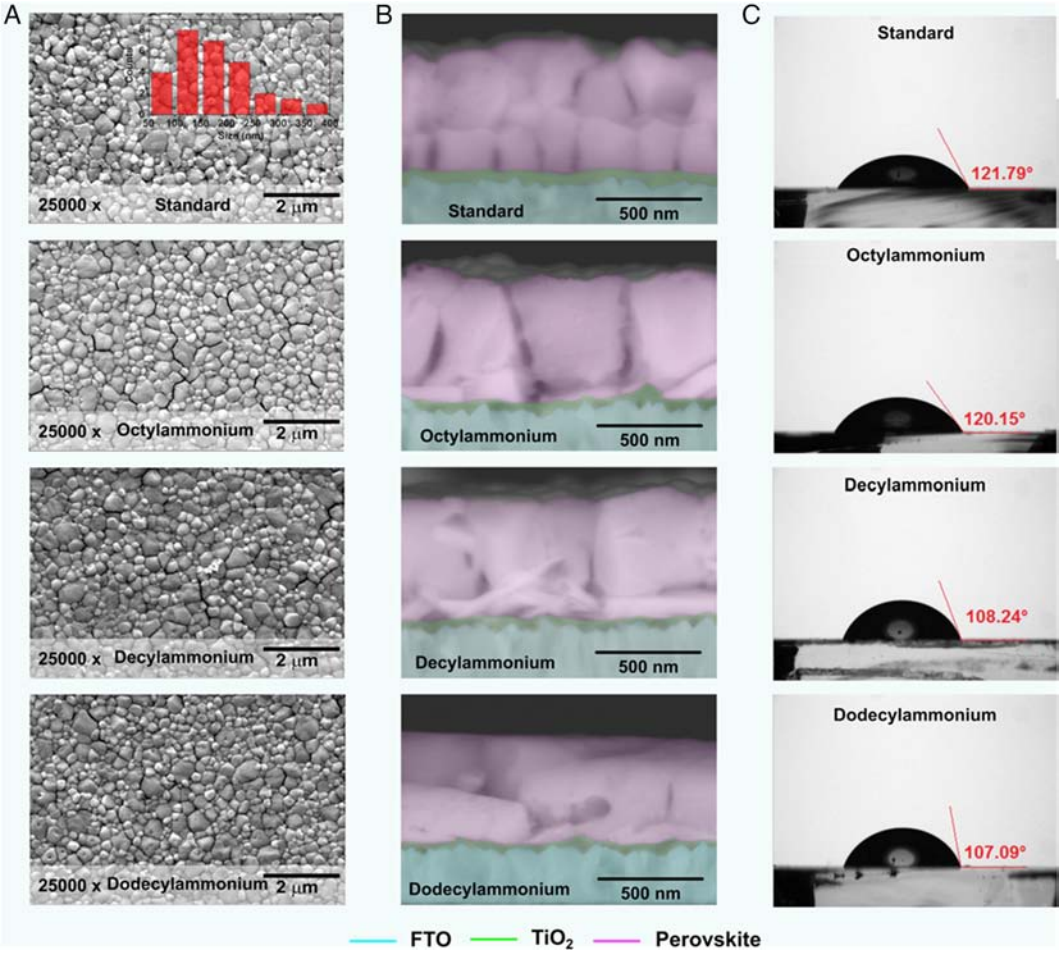


**Figure 1.** A) FEG-SEM images of the perovskite films deposited on planar $TiO_2$ substrate with and without surfactant modification with octyl, decyl, and dodecylammonium chlorides. The inset displays the crystallite size distribution of standard perovskite films. B) FEG-SEM cross-section images of perovskite films deposited on the planar substrate. C) Contact angle measurements between water drops and the surface of perovskite films on planar substrates.

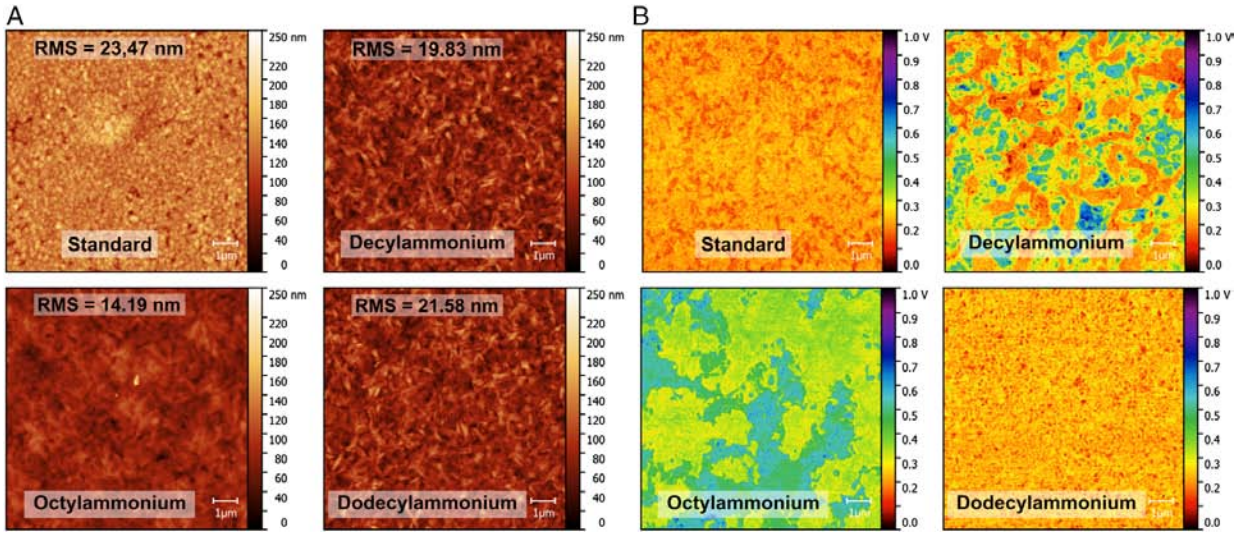


**Figure 2.** A) Atomic force microscopy images and B) Kelvin probe force microscopy image of the surface of perovskite films with and without the modification with octyl, decyl, and dodecylammonium chloride surfactants, respectively.

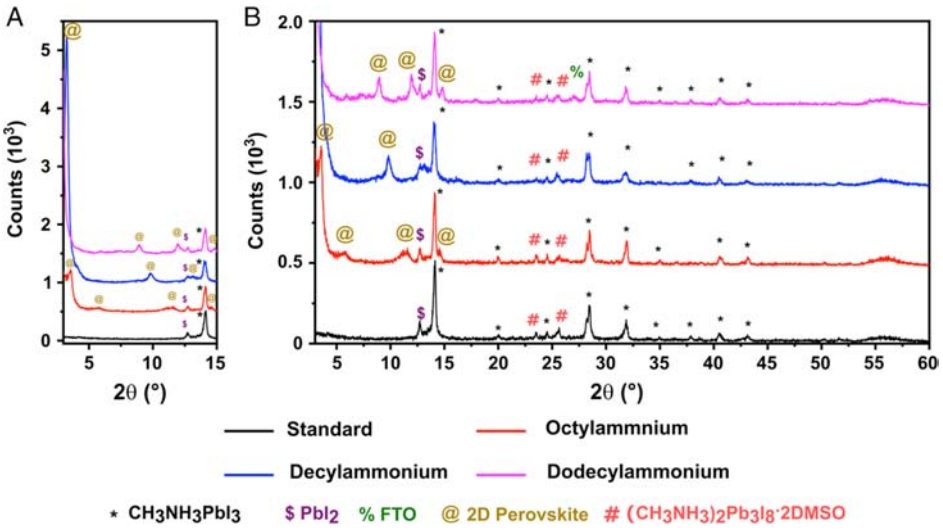


**Figure 3.** XRD patterns of $CH_3NH_3PbI_3$ films deposited over planar $TiO_2$ substrate before and after the modification with the surfactants. Focus on $2\theta$ A) from 2.5° to 15° and B) from 3° to 60°.

at $2\theta = 12.72°$ related to the presence of $PbI_2$, while peaks at $2\theta = 14.14°$, 20.02°, 24.60°, 28.32°, 31.78°, 35.21°, 39.16°, 40.64°, 43.20°, 50,32°, 51.64°, and 54.72° correspond to the planes (100), (110), (111), (200), (210), (211), (220), (221), (310), (222), (320), and (321) of the tetragonal perovskite structure. Peaks related to the structure of the fluorine-doped tin oxide (FTO) substrate are also observed at 26.60°, 33.81°, and 37.90°.[37,38] Other peaks at 7.34°, 9.30°, 21.94°, and 25.36° are related to the intermediate $(CH_3NH_3)_2Pb_3I_8{\cdot}2DMSO$ complexes, and the presence of these peaks may indicate an incomplete conversion to the perovskite tetragonal phase.[39]

By taking a close look into the X-ray diffractograms of the surfactant-modified films, it is possible to observe the presence of new peaks in the region between 2.5° and 15° (Figure 3A), related to in situ formation of 2D structures. These peaks are reflections from the (001) plane and carry information about the interlayer spacing in 2D Ruddlesden–Popper structure ($A'_2A_{m-1}B_mX_{3m+1}$). More recently, Jung et al. reported that starting with octylammonium-modified $CH_3NH_3PbI_3$, they did not form 2D structures only wrapping individual 3D perovskite grains.[40] Using the parameters proposed by Takeoka et al.[22] for chain length (0.947 nm for octylammonium chain, 1.068 nm for decylammonium, and 1.18 nm for dodecylammonium) and the thickness of perovskite sheet (0.43 nm) on the well, we can calculate the theoretical, $2\theta$ position of the (001) plane and the *d*-spacing using the Bragg's law

$$2d \sin\theta = \lambda n' \tag{4}$$

An excellent correlation between the experimental and the calculated $2\theta$ peaks is observed (**Table 1**, **2**, and **3**). Combining the information obtained using Bragg's law with the general chemical formula, we speculate that the layers, *m*, which compose the in situ 2D structures have one, two, and three sheets in the case of modification with octylammonium ($(CH_3(CH_2)_7NH_3)_2PbI_4{\cdot}(CH_3(CH_2)_7NH_3)_2(CH_3NH_3)Pb_2I_7{\cdot}(CH_3(CH_2)_7NH_3)(CH_3NH_3)_2Pb_3I_{10}$), one sheet when the decylammonium chloride was used ($((CH_3(CH_2)_9NH_3)_2PbI_4$), and two sheets in the case of the decylammonium chloride. The perovskite formation was not completed when the deposition was performed on $TiO_2$ mesoscopic substrates (Figure S2, Supporting Information). Even using the same methodology, a more intense peak of $PbI_2$ compared with planar perovskita is observed at 12.72° in all samples. The peaks related to the formation of the 2D structures are also present and also lead to the formation of layers composed of one or three sheets when modified with octylammonium and a single

**Table 1.** Theoretical and experimental crystallographic data for the perovskite film modified with octylammonium chloride, where *m* is the number of sheets in a layer, *n'* is the order of reflection, and *d* is interplanar distance.

| *m* | *d* [nm] Theoretical | *n'* | $2\theta$ Theoretical | $2\theta$ Experimental | d [nm] Experimental | Structure |
|---|---|---|---|---|---|---|
| 1 | 2.23 | 1 | 3.80 | 3.84 | $2.29 \pm 0.06$ | $(CH_3(CH_2)_7NH_3)_2PbI_4$ |
| | | 2 | 7.61 | 7.50 | | |
| | | 3 | 11.43 | 11.88 | | |
| 2 | 2.75 | 1 | 3.20 | 3.10 | $2.86 \pm 0.02$ | $(CH_3(CH_2)_7NH_3)_2$ |
| | | 2 | 6.41 | 6.12 | | $(CH_3NH_3)Pb_2I_7$ |
| 3 | 3.18 | 4 | 11.10 | 11.25 | 3.14 | $(CH_3(CH_2)_7NH_3)$ $(CH_3NH_3)_2Pb_3I_{10}$ |

**Table 2.** Theoretical and experimental crystallographic data for the perovskite film modified with decylammonium chloride, where $m$ is the number of sheets in a layer, $n'$ is the order of reflection, and $d$ is interplanar distance.

| $m$ | $d$ [nm] Theoretical | $n'$ | $2\theta$ Theoretical | $2\theta$ Experimental | $d$ [nm] Experimental | Structure |
|---|---|---|---|---|---|---|
| 1 | 2.56 | 1 | 3.44 | 3.54 | $2.71 \pm 0.10$ | $(CH_3(CH_2)_9NH_3)_2PbI_4$ |
| | | 3 | 10.32 | 9.90 | | |
| | | 4 | 13.78 | 13.18 | | |
| | | 5 | 17.25 | 16.14 | | |
| | | 9 | 31.33 | 27.06 | | |

**Table 3.** Theoretical and experimental crystallographic data for the perovskite film modified with dodecylammonium chloride, where $m$ is the number of sheets in a layer, $n$' is the order of reflection, and $d$ is interplanar distance.

| $m$ | $d$ [nm] Theoretical | $n'$ | $2\theta$ Theoretical | $2\theta$ Experimental | $d$ [nm] Experimental | Structure |
|---|---|---|---|---|---|---|
| 1 | 2.79 | 1 | 3.16 | 3.14 | $2.93 \pm 0.02$ | $(CH_3(CH_2)_{11}NH_3)_2PbI_4$ |
| | | 2 | 6.32 | 6.14 | | |
| | | 3 | 9.48 | 9.04 | | |
| | | 4 | 12.67 | 12.08 | | |
| | | 5 | 15.86 | 15.02 | | |
| | | 9 | 28.76 | 27.06 | | |
| | | 10 | 32.04 | 30.14 | | |
| 2 | 3.13 | 3 | 8.46 | 7.80 | $3.37 \pm 0.03$ | $(CH_3(CH_2)_{11}NH_3)_2(CH_3NH_3)Pb_2I_7$ |
| | | 9 | 25.57 | 23.64 | | |
| | | 10 | 28.47 | 26.68 | | |

sheet when modified with decylammonium and dodecylammonium chlorides (Table S1, S2, and S3, Supporting Information).

The electronic absorption spectra of the perovskite films (**Figure 4**A) display a small blue shift in the bandgap because of the exciton quantum confinement of the 2D structures. The bandgap of the perovskite films was estimated using the Tauc Plot (Figure 4B), where the absorption coefficient ($\alpha$) can be calculated by

$$\alpha = \frac{2.303 \times A}{t} \tag{5}$$

where $A$ is the absorbance and $t$ is the film thickness.[41,42] The bandgap values show a small increase; the bulk perovskite sample presents a value of 1.60 eV, and the octylammonium, decylammonium, and dodecylammonium films present only a small change in the bandgap values: 1.60, 1.61, and 1.61 eV, respectively.

The PL spectra were performed using a 442 nm laser; it is expected that the laser penetrates only 65 nm on the perovskite films deposited on planar $TiO_2$ substrate (Figure 4A), presenting information about the surface of the films.[43] It was possible to notice a slightly blue shift when the value of $m$ (well thickness) decreases, a consequence of the formation of in situ 2D structures into 3D bulk perovskites.[19,31,44,45] Also, the increase in the emission intensity observed after surfactant addition is a consequence of a decrease in the charge transfer rate to the $TiO_2$ film. This information allows us to infer that the presence of the surfactant is more difficult for the charges to be extracted from the 2D + 3D mixed perovskite material. Finally, it was possible to identify the formation of emission bands between 550 and 675 nm, related to the emission of the in situ–formed 2D structures as presented by Cao et al., where the main absorption band shifts to smaller wavelengths as the thickness of the layer decreases.[44] The blue shift observed in the PL spectra of perovskite films deposited on a planar substrate was also observed when the films were deposited on a mesoscopic substrate (Figure S3, Supporting Information). The intensity of the emissions, however, was higher when the films are on planar $TiO_2$ substrates.

PL decays (Figure 4C) exhibit a multiexponential profile, even for the nonmodified perovskite film, which can be adjusted using a triexponential decay equation. In addition, the formation of 2D structures in situ on the 3D perovskite film is not a controlled event, leading a complex emission dynamics. Taking into account these observations, we calculated the average emission lifetimes ($<\tau>$) to understand the charge carrier dynamics: an enhancement of the $<\tau>$ was noticed with the increase in the carbon chain length of the surfactants, from 40 ns calculated to the pristine perovskite to 44, 55, and 53 ns for the films modified with octylammonium, decylammonium, and dodecylammonium chlorides, respectively. The increase in PL lifetime is directly correlated to a decrease in nonradiative recombination processes due to surfactant modification.[46] Figure 1 shows that with the increase in alkyl chain length, more pronounced is the coalescence effect, and the film modified with

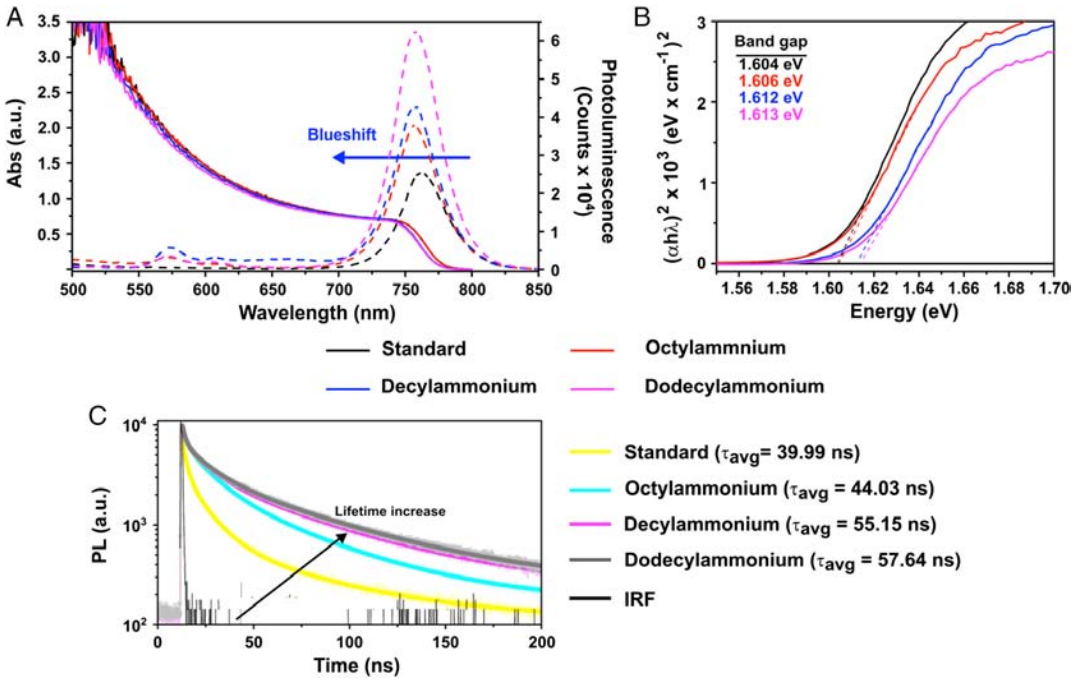


**Figure 4.** A) Normalized UV–vis and PL spectra and B) Tauc plots of the perovskite films deposited on planar $TiO_2$ substrate with and without modification. C) PL decay of different perovskite films with the average lifetimes.

dodecylammonium chloride is indeed the most compact one with larger grains. It is well established in the literature that the formation of 2D structures reduces the dominant mechanism for recombination (trap-assisted nonradiative recombination) by passivating the surface imperfections present on the 3D structure, leading to an increase in the observed lifetime by a heterojunction formation between 3D and 2D phases.[29,46–49] In our work, however, we believe that the increase in compactness and in the size of grains represents the major contribution in PL lifetime.

Perovskite films, with and without the modification, were left 21 days exposed to ambient conditions of humidity ($51.3\% \pm 5.6\%$) and temperature ($23.1 \pm 0.3\,^{\circ}C$). Visually, the moisture-induced degradation converts the brown $CH_3NH_3PbI_3$ cubic perovskite to yellow $PbI_2$ film in less than 21 days, as shown in **Figure 5**A. In the modified samples, the presence of brown spots that dispersed in a yellow background of lead iodide indicates regions where degradation is delayed.

The degradation of the films was followed by XRD (Figure 5B) and UV–vis spectroscopy measurements (Figure 5C). The reduction in the intensity of the (100) peak at $2\theta$ 14.14°, characteristic of cubic $CH_3NH_3PbI_3$, and the increase in peak intensity at $2\theta$ 12.80°, characteristic of $PbI_2$, are observed in all samples as a consequence of film degradation. In the standard perovskite film, no signal of the (100) peak is observable after 21 days. However, when the surfactants were introduced, especially in the films modified with octylammonium, the intensity of the (100) peak remains even after this period.

During this period, new peaks emerge and they can be associated with the in situ formation of 2D perovskites $(Surfactant)_2(CH_3NH_3)_{m-1}Pb_mI_{3m+1}$ $(A'_2A_{m-1}B_mX_{3m+1})$ structures with $m = 3$ and 4 for octylammonium, $m = 4$ for decylammonium and $m = 6$ for dodecylammonium. The peaks related to these structures were not initially present due to their low intensity; however, when the system undergoes degradation, they became more pronounced. The presence of these 2D structures can also be confirmed by the presence of excitonic bands in the UV–vis spectra after 7 days. In fact, after degradation, the bands associated with 3D structures give place to the bands related to 2D structures.[49] One important conclusion here is that our results suggest that there is no correlation between the surface hydrophobicity caused by the covering with the surfactant and the tolerance to moisture, since the order of hydrophobicity (dodecylammonium > decylammonium > octylammonium > standard) does not match with the order of stability observed for the perovskite films (octylammonium > decylammonium > dodecylammonium > standard).

By the XRD patterns and UV–vis spectra collected throughout 21 days, it was possible to observe that the degradation of modified perovskite films was accelerated when the perovskite films were deposited on the $TiO_2$ mesoscopic substrate. The reason for that is still unclear but might be associated with the uncompleted conversion of the precursors into perovskite using the two-step methodology. In fact, Petrus et al.[50] prepared $CH_3NH_3PbI_3$ films in an analogous way and the authors used the sequential deposition method to study the stability of these samples. In both cases, the incomplete conversion of $PbI_2$ into the perovskite phase led to a residual $PbI_2$ interlayer between $TiO_2$ and perovskite, which was reported to accelerate the film degradation.

Considering that the modification with octylammonium chloride resulted in films with improved moisture stability, we applied this film in planar PSCs with the following architecture:

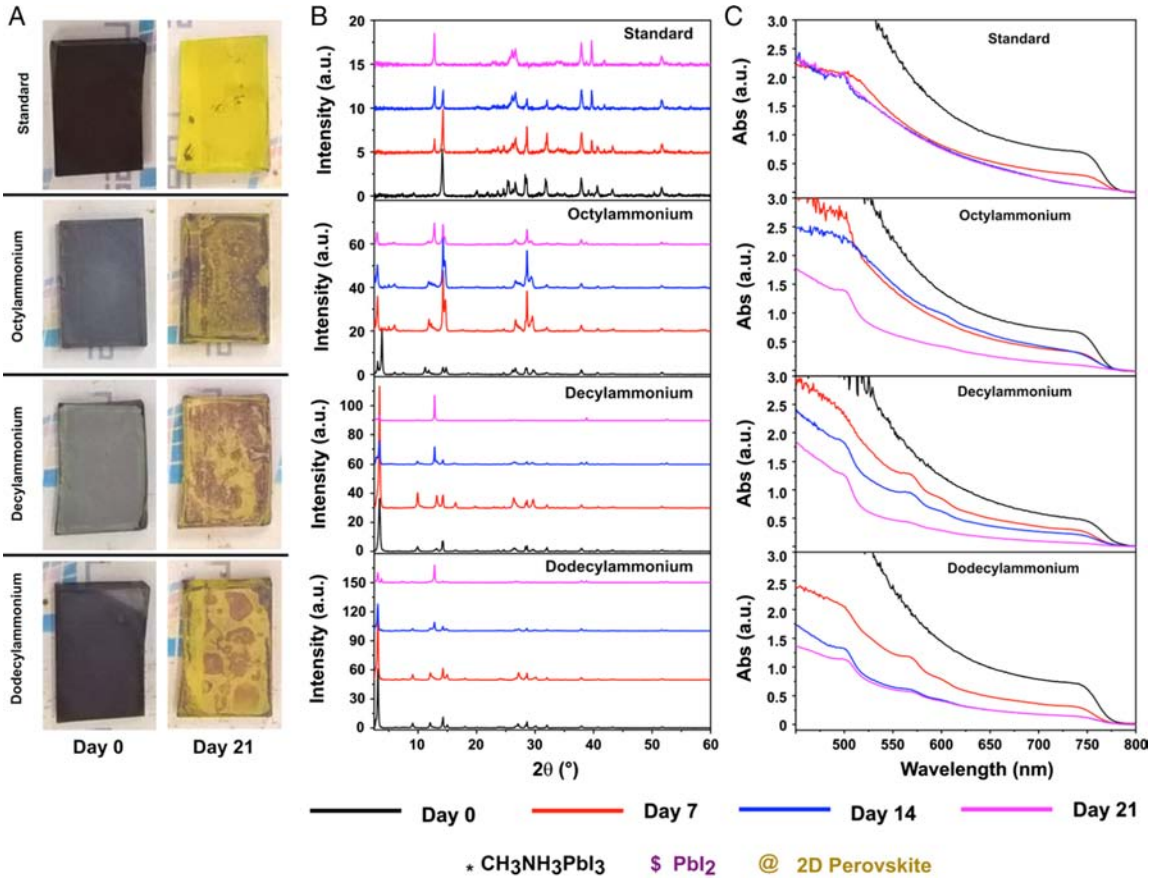


**Figure 5.** A) Photographs of the perovskite films showing the degradation patterns of perovskite films deposited over the planar substrate after 21 days of exposure to environmental conditions. B) XRD and C) UV–vis spectra of perovskite films deposited over the planar substrate, with and without the modification, at the beginning and after 7, 14, and 21 days of exposure to environmental conditions.

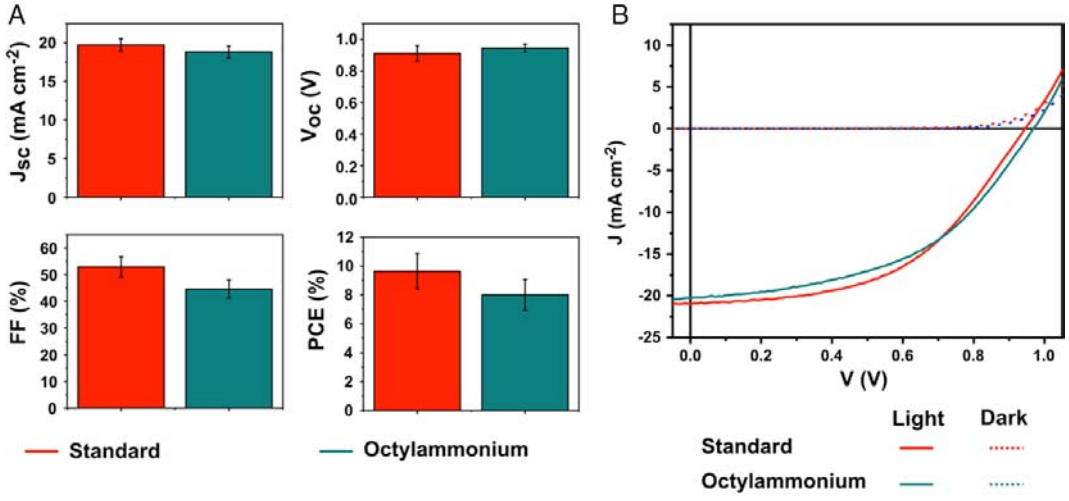


**Figure 6.** A) Devices parameters ($J_{sc}$, $V_{oc}$, FF, and PCE) of solar cells prepared without and with the modification with octylammonium chloride. B) $J \times V$ curve of the champion's devices.

FTO/compact/$TiO_2$ planar/mixed 2D + 3D perovskite/Spiro-OMeTAD/Au. Devices with the modification presented PCE of 8.00% ± 1.06% in contrast to 9.63% ± 1.21% delivered by the standard device (**Figure 6**A). A slight increase in $V_{oc}$ is observed after the perovskite modification with the octylammonium chloride surfactant (from 0.91 ± 0.04 to 0.94 ± 0.02 V): a

behavior directly linked to the enhancement of the charge carrier lifetime, which agrees to the steady-state and time-resolved domain PL measurements.

Although the $V_{OC}$ is lower than other reports in the literature for planar PSCs, the fill factor of the devices is the parameter that is most negatively affected in our studies. The values of the series resistance ($R_s$), referring to the conductivity related to the charge mobility, and the shunt resistance ($R_{sh}$), expressing the loss by recombination of the charge carriers, particularly on the interfaces were calculated to get a deeper understanding of the poor device's performance. These values can be estimated by the analysis of the variation of the current by the potential (Figure 6B) through the following equations

$$R_{sh} = \left(\frac{dV}{dI}\right)_{v=0} \quad (6)$$

$$R_s = \left(\frac{dV}{dI}\right)_{I=0} \quad (7)$$

It is important to notice that, on state-of-art devices, $R_s \rightarrow 0$ and $R_{sh} \rightarrow \infty$. The calculated values of the resistances are displayed in **Table 4**. The values of $R_s$ slightly increase with the modification, while the shunt resistance decreases by 1.5 times, after the modification. This is an indication that the poor FF values reflect an increase in the resistance due to the long chains present in the 2D structures and an increase in charge recombination at 2D + 3D interfaces. As demonstrated by Petrus et. al., the preferred orientation of the 2D structures is fundamental for charge collection; thus, more controlled deposition is required using the protocol described herein.[50]

Devices assembled with standard and modified perovskite films were subjected to stability tests. The devices were left inside the glove box for 80 h without any significant changes in PCE. Thus, we carried out an accelerated degradation test, and the results are displayed as blue stripes in **Figure 7**. The modified octylammonium–based solar cells present a smaller PCE decrease when compared with the standard device. Considering only the accelerated degradation steps (inset in Figure 7), an increase of 17.66% in the lifetime of the devices based on octylammonium-modified films was observed. These results agree with the improved moisture stability induced by the presence of 2D structures.

## 3. Conclusions

In this work, we successfully prepared mixed 2D + 3D perovskite in situ by dripping long chain alkylammonium chloride surfactants (octylammonium, decylammonium, and dodecylammonium) on perovskite films. The chosen methodology induces the formation of 2D structures from 3D polycrystalline $CH_3NH_3PbI_3$ but does not allow selectivity in the number of the layers. A small blue shift in the absorption and PL spectra indicates a decrease in the bandgap, and an increase in the charge carrier lifetime was observed on the films after the modification with alkylammonium. The modified films are more tolerant to humidity than the standard films because of the presence of the 2D structures; however, the hydrophobicity order does not match the results of the stability test on modified films.

The modification proposed, however, has led to a reduction of 26.00% (FB) and 17.92% on the PCE of devices, which are related to charge recombination on the interfaces. The modified devices presented a lifetime of 17.66% greater than those assembled without the proposed modification when both were exposed to accelerated degradation tests.

**Table 4.** Values for series and shunt resistance in standard cells and modified with octylammonium chloride.

| | $R_s$ ($\Omega\,cm^{-2}$) | $R_{sh}$ ($\Omega\,cm^{-2}$) |
|---|---|---|
| Standard | 11.95 | 581.52 |
| Octylammonium | 14.00 | 384.95 |

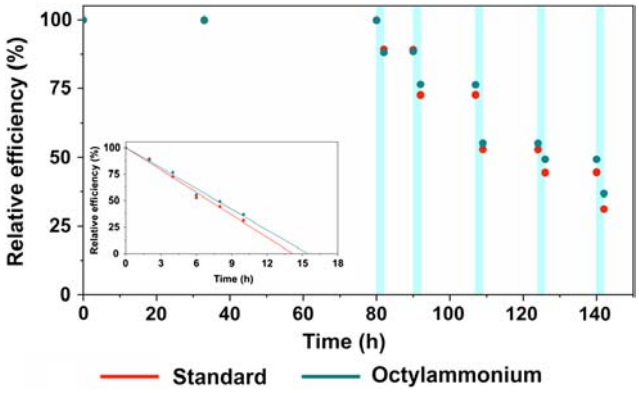


**Figure 7.** Efficiency loss related to the degradation of the device by exposing the devices to ambient temperature and humidity conditions.

## 4. Experimental Section

*Preparation of Methylammonium Iodide*: Methylamine (8.65 mL) and iodidric acid (HI) (13.19 mL) were added to a 50 mL round-bottommed flask. The mixture was kept under reflux in an ice bath and under constant stirring. After 2 h of reaction, the mixture was filtered, and the filtrate was dissolved in a small volume of hot ethanol and recrystallized from ice-cold ethyl ether. After recrystallization, the material was dried in a vacuum oven for 24 h at 100 °C. The dried material was stored under vacuum to avoid water adsorption.

*Preparation of Alkylammonium Chloride*: Equimolar amounts of the alkylamine compounds (octylamine, decylamine, and dodecylamine) and hydrochloric acid were added in round-bottomed flasks, which were placed in an ice bath and under constant stirring (the acid was slowly added to avoid accidents). After 2 h of reaction, the mixture was filtered, and the solids were dissolved in a small volume of hot ethanol and recrystallized from ice-cold ethyl ether. After purification, the material was dried in a vacuum oven for 24 h at 100 °C. The dried material was stored under vacuum to avoid water absorption.

*Preparation of Substrates*: FTO-coated glasses were cut into rectangles of 12.5 mm by 18.75 mm, and an FTO region of 18.75 mm by 2.00 mm, near the edge, was removed using zinc and hydrochloric acid (2 mol $L^{-1}$). The substrate was then washed and sonicated sequentially in detergent/water, distilled water, ethanol, and isopropanol and finally oven dried at 100 °C for 2 h. Subsequently, the substrates were then treated with ozone for 30 min prior to deposition of the following layers.

*Deposition of $TiO_2$ Films*: $TiO_2$ films were deposited in both planar and mesoscopic configurations. A solution of 73.2 µL $mL^{-1}$ of titanium diisopropoxide bis (acetylacetonate) in 1-butanol was used to prepare the

planar configuration. The deposition was performed by the spin-casting method at 2000 RPM for 30 s. The film was heated at 125 °C for 5 min, and after cooling at room temperature, it was treated with ozone. This procedure was repeated a second time, and after deposition, the film was thermally treated at 500 °C for 30 min. The deposition and treatment of the $TiO_2$ films was carried out in ambient conditions.

The mesoscopic film was deposited over the compact $TiO_2$ layer as previously described without the final thermal treatment. A porous layer was then deposited using a dispersion of $TiO_2$ nanoparticles (149 mg of 20 nm nanoparticle paste from DyeSol DSL 18NR-T) in 1 ml of ethanol previously stirred for 30 min. The mesoporous film was deposited by the spin-casting method at 5000 RPM for 30 s. Finally, the substrate was heated at 500 °C for 30 min.

*Deposition of Perovskite Films*: The perovskite layer was prepared using a two-step methodology using solutions of MA iodide in isopropanol (30 mg $mL^{-1}$) and lead iodide in dimethylformamide (DMF):dimethylsulphoxide (DMSO) (17:3, v/v) (645.4 mg $mL^{-1}$) as precursors. The preparation of the solutions as well the deposition of the perovskite films was performed inside a glove box with $N_2$: 1) The lead iodide solution was dripped onto the substrate, which was then rotated at 4000 RPM for 30 s; 2) The substrate was accelerated to 6000 RPM for 30 s for film drying; 3) The substrate was decelerated at 5000 RPM for 35 s. After stabilization of the rotation speed, methylammonium iodide (MAI) solution was dripped at a rate of 1 drop every 1.25 s. At this stage, the formation of the perovskite film occurs; 4) Deceleration up to 3000 RPM where the substrates are held for 10 s to ensure solvent removal and drying; 5) Finally, the films were heated at 100 °C for 60 min.

*Modification of the Perovskite*: Modification of the perovskite films was performed using alkylammonium chlorides of different chain lengths ($n = 8$, 10, and 12 carbons). Previously, the surfactants were solubilized in chloroform at a concentration of $4.5 \times 10^{-5}$ mol $L^{-1}$. Then, 800 µL solution was rapidly dripped onto the surface of perovskite films previously rotated at 2000 RPM. After 20 s of rotation, 20 µL of pure chloroform was dripped to wash up the excess of surfactant. The modification was also performed inside a glove box.

*Deposition of the Hole Transport Layer*: N2, N2, N2′, N7, N7, N7′, N7′-octakis(4-methoxyphenyl)-9,9′-spirobi[9H-fluorene]-2,2′,7,7′-tetramine (Spiro-OMeTAD) was deposited on the perovskite as a hole transport layer (HTL). The film was deposited by a spin-casting method inside the glove box, at 3000 RPM for 45 s, using 30 µL of a 0.068 mol $L^{-1}$ solution of Spiro-OMeTAD in chlorobenzene with the addition of 16.1 µL $mL^{-1}$ of 4-tert-butylpyridine (TBP) and 30.4 µl $mL^{-1}$ of a solution of lithium bis(trifluoromethanesulfonyl)imide (LiTSFI) in acetonitrile (170 mg $mL^{-1}$). The film was then kept for 48 h in a dry chamber to increase the conductivity by a slow oxidation process. Finally, 60 nm thick film of gold was deposited as the top electrode to complete the assembly of the solar cells. The deposition was performed by ultravacuum thermal evaporation at 1 Å $s^{-1}$ inside the glove box.

*Field Emission Scanning Electron Microscopy*: Images of the films were acquired using a scanning electron microscope, JEOL, model 6360LV, with beam energy of 5 kV.

*X-Ray Diffraction*: X-ray diffractograms of the perovskite films with and without modification were obtained on a Shimadzu diffractometer, model XRD-6000 with Cu Kα radiation of 0.154 nm wavelength.

*Preparation of Samples for Photophysical Measurements*: The perovskite films with and without modifications were assembled in a clean glass substrate in the same way of the photovoltaic devices.

*Visible and UV Spectroscopy (UV–vis)*: Absorption spectra of the perovskite films with and without modification were acquired using an Agilent spectrophotometer, model Cary 60, in the 500–800 nm range.

*Photoluminescence Spectroscopy*: PL spectra of the perovskite films with and without modification were acquired using as a source of excitation a 300 W Kimmon He-Cd laser with a wavelength of 442 nm and an Ocean Optics USB2000+ detector with a homemade laboratory software based on LabView.

*Time-Resolved Photoluminescence Spectroscopy*: Charge carrier emission dynamics of the 2D/3D perovskites films were acquired using a time-correlated single-photon counting (TCSPC) in an Edinburg Analytical Instruments FL 900 spectrofluorimeter with an MCP-PMT (Hamamatsu R3809U-50) with a PicoQuant pulsed laser operating at $\lambda_{exc} = 440$ nm (model LDH-D-C-440, with a bandwidth of 10 nm, pulses <100 ps, $P = 50$ mW). The decay signals were collected at the maximum emission wavelength of the perovskite film. The instrument response was recorded using Ludox samples. At least 10 000 counts in the peak channel were accumulated for the lifetime determination. The emission decays were analyzed using exponential functions as described previously.[51]

*Contact Angle's Measurement*: High-definition photographs were acquired immediately after the drip of water on the surface of the films to determine the hydrophilic properties. As the contact angle formed between the water drop and the surface decreases, the hydrophobicity increases. Such measurements were performed using an Attension optical tensiometer, Theta model.

*Stability Tests*: The films were left exposed to ambient conditions (temperature between 22 and 24 °C and humidity in the range of 40–60%) to evaluate the stability of the perovskite with and without modification. The ambient conditions were periodically monitored with a thermohygrometer during 3 weeks. At the end of each week, XRD and UV–vis spectra were obtained to evaluate the presence of degraded species and the formation of 2D structures.

*Kelvin and Atomic Force Microscopies*: The morphology of the perovskite films with and without modification was evaluated using an NX10 atomic force microscope (AFM) from Prak Systems. Together with surface imaging, surface potential measurements were performed using a Kelvin probe. A pointprobe-plus Silicon-SPM-Sensor (PPP-EFM-W) with a resistivity of 0.01–0.02 Ω cm produced by nanosensors was used for this purpose.

*Characterization of the Devices*: All devices were characterized with a Sciencetech class AAA solar simulator, calibrated with a silicon reference solar cell with a KG5 filter, with 1.5G AM at 100 mW $cm^2$. The current density curves versus (*J–V*) were acquired in a Keithley 2400 SourceMeter, with steps of 10 mV and delay time of 0.25 s, resulting in 40 mV $s^{-1}$ of scan rate.

*Stability Tests*: The devices without sealing were left inside the glove box for 80 h and periodically with the PCE measured. Then, after different periods, they were then removed from the glove box and exposed to ambient conditions (humidity of 51.3% ± 5.6% and temperature of 23.1 ± 0.3 °C) for 2 h to increase the degradation and then, placed in the glove box again so the PCE could be measured.

## Supporting Information

Supporting Information is available from the Wiley Online Library or from the author.

## Acknowledgements

The authors acknowledge FAPESP, CNPq, CAPES, INEO, and Brazilian Nanotechnology National Laboratory LNNano for financial and technical support. R.S. thanks the Sao Paulo Research Foundation (FAPESP, Grant 2017/12582-5, and 2013/16245-2). A. F. N gratefully acknowledges support from FAPESP (Grant 2017/11986-5) and Shell and the strategic importance of the support given by ANP (Brazil's National Oil, Natural Gas and Biofuels Agency) through the R&D levy regulation.

## Conflict of Interest

The authors declare no conflict of interest.

## Keywords

energy conversion, perovskite solar cells, photovoltaics, stability, 2D perovskite

Received: May 13, 2019
Revised: June 15, 2019
Published online:

[1] A. Kojima, K. Teshima, Y. Shirai, T. Miyasaka, *J. Am. Chem. Soc.* **2009**, *131*, 6050
[2] NREL (**2018**) Efficiency chart.
[3] S. A. Kulkarni, T. Baikie, P. P. Boix, N. Yantara, N. Mathews, S. Mhaisalkar, *J. Mater. Chem. A* **2014**, *2*, 9221.
[4] N. Pellet, P. Gao, G. Gregori, T. Y. Yang, M. K. Nazeeruddin, J. Maier, M. Grätzel, *Angew. Chemie Int. Ed.* **2014**, *53*, 3151
[5] M. Saliba, T. Matsui, J.-Y. Seo, K. Domanski, J.-P. Correa-Baena, M. K. Nazeeruddin, S. M. Zakeeruddin, W. Tress, A. Abate, A. Hagfeldt, M. Grätzel, *Energy Environ. Sci.* **2016**, *9*, 1989.
[6] M. I. Dar, G. Jacopin, S. Meloni, A. Mattoni, N. Arora, A. Boziki, S. M. Zakeeruddin, U. Rothlisberger, M. Grätzel, *Sci. Adv.* **2016**, *2*, e1601156.
[7] J. H. Noh, S. H. Im, J. H. Heo, T. N. Mandal, S. I. Seok, Nano Lett. **2013**, *13*, 1764.
[8] S. D. Stranks, G. E. Eperon, G. Grancini, C. Menelaou, M. J. P. Alcocer, T. Leijtens, L. M. Herz, A. Petrozza, H. J. Snaith, *Science*, **2013**, *342*, 341.
[9] G. Xing, N. Mathews, S. Sun, S. S. Lim, Y. M. Lam, M. Grätzel, S. Mhaisalkar, T. C. Sum, *Science*, **2013**, *342*, 344.
[10] S. De Wolf, J. Holovsky, S.-J. Moon, P. Löper, B. Niesen, M. Ledinsky, F.-J. Haug, J.-H. Yum, C. Ballif, *J. Phys. Chem. Lett.* **2014**, *5*, 1035.
[11] D. Shi, V. Adinolfi, R. Comin, M. Yuan, E. Alarousu, A. Buin, Y. Chen, S. Hoogland, A. Rothenberger, K. Katsiev, Y. Losovyj, X. Zhang, P. A. Dowben, O. F. Mohammed, E. H. Sargent, O. M. Bakr, *Science*, **2015**, *347*, 519.
[12] S. Yang, Y. Wang, P. Liu, Y.-B. Cheng, H. J. Zhao, H. G. Yang, *Nat. Energy*, **2016**, *1*, 15016.
[13] J. You, Y. Yang, Z. Hong, T.-B. Song, L. Meng, Y. Liu, C. Jiang, H. Zhou, W.-H. Chang, G. Li, Y. Yang, *Appl. Phys. Lett*, **2014**, *105*, 183902.
[14] I. Hwang, I. Jeong, J. Lee, M. J. Ko, K. Yong, *ACS Appl. Mater. Interfaces*, **2015**, *7*, 17330.
[15] C. Müller, T. Glaser, M. Plogmeyer, M. Sendner, S. Döring, A. A. Bakulin, C. Brzuska, R. Scheer, M. S. Pshenichnikov, W. Kowalsky, A. Pucci, R. Lovrinčić, *Chem. Mater.* **2015**, *27*, 7835.
[16] J. M. Howard, E. M. Tennyson, S. Barik, R. Szostak., E. Waks, M. F. Toney, A. F. Nogueira, B. R. A. Neves, M. S. Leite, *J. Phys. Chem. Lett.* **2018**, *9*, 3463.
[17] T. M. Koh, K. Thirumal, H. S. Soo, N. Mathews, *ChemSusChem*, **2016**, *9*, 2541.
[18] C. C. Stoumpos, D. H. Cao, D. J. Clark, J. Young, J. M. Rondinelli, J. I. Jang, J. T. Hupp, M. G. Kanatzidis, *Chem. Mater.* **2016**, *28*, 2852.
[19] C. M. M. Soe, W. Nie, C. C. Stoumpos, H. Tsai, J. C. Blancon, F. Liu, J. Even, T. J. Marks, A. D. Mohite, M. G. Kanatzidis, *Adv. Energy Mater.* **2018**, *8*, 2.
[20] G. Grancini, C. Roldán-Carmona, I. Zimmermann, E. Mosconi, X. Lee, D. Martineau, S. Narbey, F. Oswald, F. De Angelis, M. Graetzel, M. K. Nazeeruddin, *Nat. Commun.* **2017**, *8*, 1.
[21] A. Vassilakopoulou, D. Papadatos, I. Zakouras, I. Koutselas, *J. Alloys Compd.* **2017**, *692*, 589.
[22] Y. Takeoka, K. Asai, M. Rikukawa, K. Sanui, *Bull. Chem. Soc. Jpn.*, **2006**, *79*, 1607.
[23] L Etgar, *Energy Environ. Sci.* **2018**, *11*, 234.
[24] A. M. A. Leguy, P. Azarhoosh, M. I. Alonso, M. Campoy-Quiles, O. J. Weber, J. Yao, D. Bryant, M. T. Weller, J. Nelson, A. Walsh, M. van Schilfgaarde, P. R. F. Barnes, *Nanoscale*, **2016**, *8*, 6317.
[25] S. Ahmad, J. J. Baumberg, G. Vijaya Prakash, *J. Appl. Phys.* **2013**, *114*, 233511.
[26] L. N. Quan, M. Yuan, R. Comin, O. Voznyy, E. M. Beauregard, S. Hoogland, A. Buin, A. R. Kirmani, K. Zhao, A. Amassian, D. H. Kim, E. H. Sargent, *J. Am. Chem. Soc.* **2016**, *138*, 2649.
[27] G. Li, T. Zhang, N. Guo, F. Xu, X. Qian, Y. Zhao, *Angew. Chemie Int. Ed.* **2016**, *55*, 13460.
[28] R. K. Misra, B.-E. Cohen, L. Iagher, L. Etgar, *ChemSusChem*, **2017**, *10*, 3712.
[29] T.M. Koh, V. Shanmugam, X. Guo, S. S. Lim, O. Filonik, E. M. Herzig, P. Müller-Buschbaum, V. Swamy, S. T. Chien, S. G. Mhaisalkar, *N. Mathews. J. Mater. Chem. A*, **2018**, *6*, 2122.
[30] P. Chen, Y. Bai, S. Wang, M. Lyu, J. H. Yun, L. Wang, *Adv. Funct. Mater.* **2018**, *1706923*, 1.
[31] K. T. Cho, Y. Zhang, S. Orlandi, M. Cavazzini, I. Zimmermann, A. Lesch, N. Tabet, G. Pozzi, G. Grancini, M. K. Nazeeruddin, *Nano Lett.* **2018**, *18*, 5467.
[32] D. Gedamu, I. M. Asuo, D. Benetti, M. Basti, I. Ka, S. G. Cloutier, F. Rosei, R. Nechache, *Sci. Rep.* **2018**, *8*, 1.
[33] A. Cerdán-Pasarán, S. Sidhik, T. López-Luke, E. De la Rosa, *Sol. Energy*, **2019**, *177* 538.
[34] H. Yu, F. Wang, F. Xie, W. Li, J. Chen, N. Zhao, *Adv. Funct. Mater.* **2014**, *24*, 7102
[35] V. L. Pool, A. Gold-Parker, M. D. McGehee, M. F. Toney, *Chem. Mater*, **2015**, *27*, 7240.
[36] K. Yao, X. Wang, Y. X. Xu, F. Li, L. Zhou, *Chem. Mater.* **2016**, *28*, 3131.
[37] T. Oku, *Solar Cells—New Approaches and Reviews*, **2015**, InTech, London.
[38] T. Baikie, Y. Fang, J. M. Kadro, M. Schreyer, F. Wei, S. G. Mhaisalkar, M. Graetzel, T. J. White, *J. Mater. Chem. A*, **2013**, *1*, 5628.
[39] Y. Rong, Z. Tang, Y. Zhao, X. Zhong, S. Venkatesan, H. Graham, M. Patton, Y. Jing, A. M. Guloy, Y. Yao, *Nanoscale*, **2015**, *7*, 10595.
[40] M. Jung, T. J. Shin, J. Seo, G. Kim, S. I. Seok, *Energy Environ. Sci.* **2018**, *11*, 2188.
[41] J. Tauc, *Mater. Res. Bull.* **1968**, *3*, 37.
[42] B. N. Ezealigo, A. C. Nwanya, S. Ezugwu, S. Offiah, D. Obi, R. U. Osuji, R. Bucher, M. Maaza, P. Ejikeme, F. I. Ezema, *Arab. J. Chem*, **2017**
[43] R. Szostak, J. A. P. Castro, A. S. Marques, A. F. Nogueira, J. Photonics Energy, **2017**, *7*, 022002.
[44] D. H. Cao, C. C. Stoumpos, O. K. Farha, J. T. Hupp, M. G. Kanatzidis, *J. Am. Chem. Soc.* **2015**, *137*, 7843.
[45] D. Cortecchia, S. Neutzner, A. R. S. Kandada, E. Mosconi, D. Meggiolaro, F. De Angelis, C. Soci, A. Petrozza, *J. Am. Chem. Soc.* **2017**, *139*, 39.
[46] Z. Wang, Q. Lin, F. P. Chmiel, N. Sakai, L. M. Herz, H. J. Snaith, *Nat. Energy*, **2017**, *2*, 17135.
[47] B. Li, Y. Zhang, L. Fu, T. Yu, S. Zhou, L. Zhang, L. Yin, *Nat. Commun.* **2018**, *9*, 1076.
[48] Wang, F, W. Geng, Y. Zhou, H.-H. Fang, C.-J. Tong, M. A. Loi, L.-M. Liu, N. Zhao, *Adv. Mater.* **2016**, *28*, 9986.
[49] L. Gan, H. He, S. Li, J. Li, Z. Ye, *J. Mater. Chem. C*, **2016**, *4*, 10198.
[50] M. L. Petrus, Y. Hu, D. Moia, P. Calado, A. M. A. Leguy, P. R. F. Barnes, P. Docampo, *ChemSusChem*, **2016**, *9*, 2699.
[51] J. C. Germino, J. N. de Freitas, R. A. Domingues, F. J. Quites, M. M. Feleiros, T. D. Z. Atvars, *Synth. Met.* **2018**, *241*, 7.

 